LANGMUIR

pubs.acs.org/Langmuir Article

Quantitative Description of Bubble Formation in Response to Electrolyte Engineering

Huihang Qiu, Keisuke Obata, Zhicheng Yuan, Takeshi Nishimoto, Yaerim Lee, Keisuke Nagato, Ikuya Kinefuchi, Junichiro Shiomi, and Kazuhiro Takanabe*

Cite This: *Langmuir* 2023, 39, 4993−5001 Read Online

ACCESS | Metrics & More | Article Recommendations | Supporting Information

ABSTRACT: The green hydrogen economy is expected to play a crucial role in carbon neutrality, but industrial-scale water electrolysis requires improvements in efficiency, operation costs, and capital costs before broad deployment. Electrolysis operates at a high current density and involves the substantial formation of gaseous products from the electrode surfaces to the electrolyte, which may lead to additional resistance and a resulting loss of efficiency. A detailed clarification of the bubble departure phenomena against the electrode surface and the surrounding electrolytes is needed to further control bubbles in a water electrolyzer. This study clarifies how electrolyte properties affect the measured bubble detachment sizes from the comparisons with analytical expressions and dynamic simulations. Bubble behavior in various electrolyte solutions and operating conditions was described using various physical parameters. A quantitative relationship was then established to connect electrolyte properties and bubble departure diameters, which can help regulate the bubble management through electrolyte engineering.

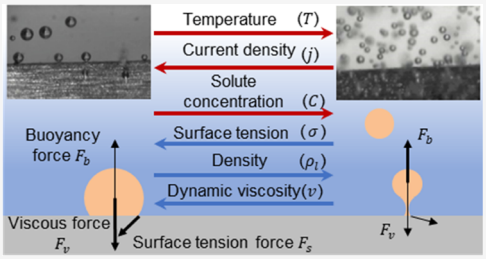

INTRODUCTION

The green economy aims to create a system that could reduce emissions of CO_2 and environmental pollutants using sustainable and efficient energy resources.[1] Hydrogen is a promising commercial fuel because it produces only water when combusted. Among various hydrogen production methods, water electrolysis has attracted considerable interest because it is a mature process and can produce green hydrogen when coupled with the electricity from renewable energy sources such as solar and wind power.

To maximize the productivity of an electrolyzer, water electrolysis is performed at high current densities that coincide with the substantial formation of gas bubbles from the electrode surface. A higher current density leads to a higher overpotential from bubble resistivity.[2−5] Iwata et al. tuned the electrode wettability to show that the bubble dynamics influence the transport overpotential to a degree comparable to the activation overpotential at a high current density.[6] Dorfi et al. found that larger bubbles attached to the electrode surface led to large experimental photocurrent losses in the photoelectrochemical water-splitting system.[5] These studies present the common efficiency losses induced by gas bubbles. Therefore, clarification of the bubble dynamics in the electrochemical system is invaluable for industrial water electrolysis.

Commonly accepted bubble-induced impacts on the overpotential can be summarized into three contributions: activation, ohmic, and concentration overpotentials.[7] The attached bubbles would screen some of the electrodes[2,3] and block the active catalytic sites,[8] thus resulting in additional activation overpotential. Meanwhile, surface-attached bubbles will induce a localized current density distribution,[2] which causes an additional ohmic overpotential. The detached bubbles will similarly create voids within the electrolyte,[9] which decreases the conductivity of the electrolyte leading to a higher ohmic overpotential. In terms of concentration, the growth and departure of gas bubbles can reduce a supersaturation level of dissolved gases. This led to convective flow that promotes mass transfer,[10] thus enhancing the efficiency of the electrolysis.[11]

Ideally, the detachment sizes of the bubbles should be so small that they will not induce any additional overpotential due to the shielding of the electrodes, while frequent detachment develops strong convective flows that improve mass transfer at high current densities.[12] Previous reports evaluated different strategies, such as active methods, including flow fields,[13] magnetic fields,[14] and acoustic fields,[15] as well as passive methods, such as designing special electrolyzer structures[16] and fabricating superhydrophilic electrode surfaces.[6,17] Iwata et al. used PTFE to modify porous nickel electrodes and found a relationship between the electrode wettability and the bubble

Received: December 29, 2022
Revised: February 28, 2023
Published: March 29, 2023

ACS Publications

© 2023 The Authors. Published by American Chemical Society

https://doi.org/10.1021/acs.langmuir.2c03488
Langmuir 2023, 39, 4993−5001

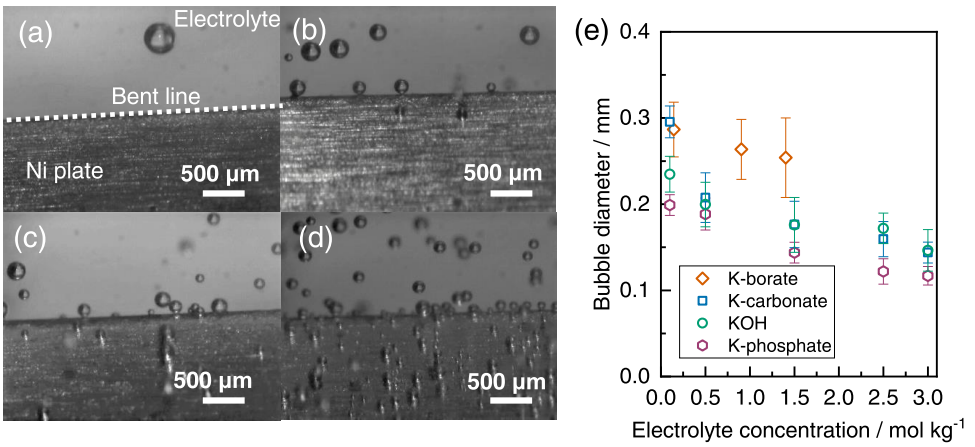

Figure 1. Oxygen bubble observation on 1 × 1 cm^2 bent nickel plate. High-speed video image of bubbles during oxygen evolution reaction (OER) with an operating current density of 50 mA cm^{-2} in (a) 0.1 mol kg^{-1}, (b) 0.5 mol kg^{-1}, (c) 1.5 mol kg^{-1}, and (d) 3.0 mol kg^{-1} carbonate buffer solutions at pH 10.5 and 298 K. The highest line of the electrode (shown as a white dashed line in panel (a)) is the bent line, where detached bubbles are counted. (e) Relationship between solute concentrations and bubble diameters, where bubble diameters were obtained from the average diameter of 15−50 bubbles departed at the bent line.

detachment radius.[6] Li et al. successfully fabricated a pine-shaped Pt electrode with superhydrophilicity that effectively reduced the bubble detachment size by reducing the bubble contact area and the bubble adhesion force.[18]

There are also some excellent theoretical studies that concentrate on the bubble behavior at the electrode surface by deducing analytical expressions and conducting simulations.[19−21] One widely applied analytical expression is the Fritz equation that was derived from the balances between buoyancy and surface tension forces on a static bubble.[22] Ma et al. reported a two-dimensional simulation study on the bubble formation and dynamics in bubble columns, thus revealing the effects of electrolyte properties on the diameters and departure time of single bubbles.[20] However, this study was limited to the two-dimensional discussion and missed the correlation between electrochemical experiments and simulations. Li et al. proposed analytical equations to predict the bubble departure diameters on micro-/nanostructured surfaces based on the three-dimensional static simulation model.[19] Clearly, progress has been achieved not only in the experimental studies but also in simulation studies.

To the best of our knowledge, however, most experimental studies still focus on controlling the wettability of electrode surfaces.[23] There are still a lack of detailed investigations into the relationship between the electrolyte physical properties and bubble departure diameters. In addition to a conventional approach to tune hydrophilicity at the electrode surface, adjusting electrolyte ions, namely, electrolyte engineering, would introduce changes in the reaction mechanism,[24] the electrode kinetics,[25] and the mass transport.[26] These concepts are further expanded in the bubble management in this study. Quantitative descriptions of the relationship between bubbles and electrolyte properties in electrochemical reactions would help to develop efficient water-splitting devices. Here, the bubble departure diameters were quantified in various electrolytes under various operating conditions such as temperature and current density using a high-speed camera during water electrolysis.

To advance the theoretical study, the results were integrated into an analytical equation that could predict bubble detachment sizes at the micropillar surface. In turn, a quantitative description was deduced to clarify the contributions from the physical properties of electrolytes and the electrode surface exposed to the operating conditions.

Most previous simulation studies concentrated on building up static computational models, where force balances were considered at given bubble diameters to determine the detachment. To further analyze the impact of dynamic factors, e.g., the viscous force, a three-dimensional dynamic model was constructed during the bubble departure process. Combining experimental and computational results, a quantitative bridge and a general trend were then established between physical properties and bubble sizes. This quantitative relationship provides the possibility of regulating bubble sizes through electrolyte engineering.

RESULTS AND DISCUSSION

Observation of Bubble Detachments in Various Electrolyte Solutions and Operating Conditions. During the oxygen evolution reaction (OER), a high-speed camera was used to record oxygen bubble detachment from the bent line of the nickel plate. (The highest line of the electrode was the bent line, where oxygen bubbles detached were counted, and the detailed experimental setup is shown in Figure S1.) Figure 1a−d shows oxygen bubble images taken during water electrolysis. The high-speed camera was tuned to focus on the bent line, where bubbles detached behind and in front of were blurred. Only those oxygen bubbles detached at the bent line were clearly observed with a sharp edge, whose diameters were obtained through ImageJ. Figure 1e shows the relationship between bubble detachment size and electrolyte solute concentration. The bubble departure diameter decreases with increasing electrolyte solute concentration. Although a relatively large error remained due to the limited number of bubbles counted from the bent line, a similar deduction trend was also seen in different electrolyte solutions, thus indicating that the influence of the solute concentration is independent of the ions. When the concentration of the potassium carbonate solution increases from 0.1 to 3.0 mol kg^{-1}, the average detached bubble diameter decreases from 290 to 140 μm. This relationship could be explained by the force imposed on the attached bubbles. One of the proposed explanations is that a

https://doi.org/10.1021/acs.langmuir.2c03488
Langmuir 2023, 39, 4993−5001

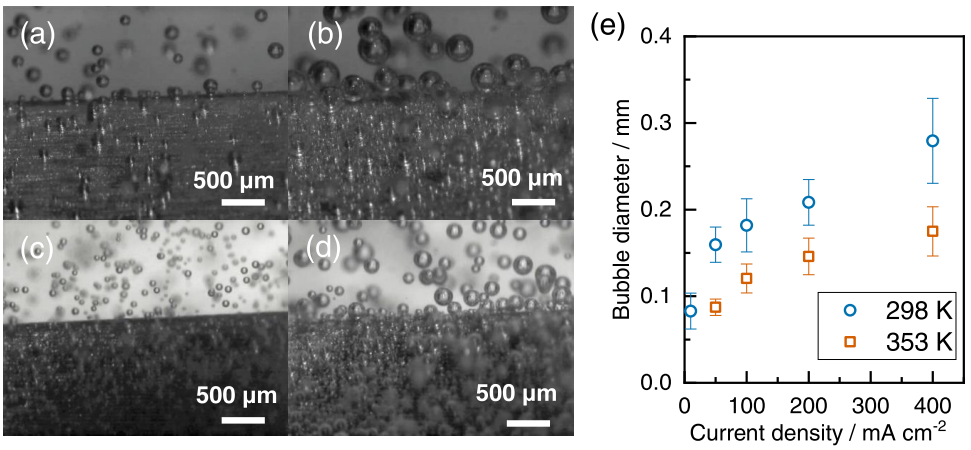

Figure 2. Oxygen bubbles on a 1 × 1 cm^2 bent nickel plate. High-speed video images of bubbles during the OER in 2.5 mol kg^{-1} carbonate buffer solution at pH 10.5 with operating conditions of (a) 50 mA cm^{-2} and 298 K, (b) 400 mA cm^{-2} and 298 K, (c) 50 mA cm^{-2} and 353 K, and (d) 400 mA cm^{-2} and 353 K. The highest line of the electrode (shown as a white dashed line in Figure 1a) is the bent line, where detached bubbles are counted. (e) Relationship between bubble diameters, current densities, and temperatures (during the observation, no bubbles detached at the bent line were recorded at 10 mA cm^{-2} and 353 K); bubble diameters were obtained from the average diameter of 15−50 bubbles that departed at the bent line.

smaller bubble departure size would occur as the interfacial tension force decreases in a dense viscous solution. Besides dynamic viscosity, many other physical properties also change with increasing solute concentration. For example, the density of the K-carbonate solution increases from 1010 to 1250 kg m^{-3}, the surface tension increases from 75 to 82 mN m^{-1}, and the dynamic viscosity increases from 0.83 to 1.9 mPa s (Figure S2). The physical properties of potassium hydroxide solutions and K-borate buffer solutions are also shown in Figure S2. The change in density, surface tension, and dynamic viscosity would also partially influence the bubble diameters. These physical properties increase linearly with increasing solute concentration in the studied concentration range (<2.5 mol kg^{-1}). Thus, bubbles can be represented as the function of solute concentration in this concentration range. Their values can be roughly estimated from the solute concentration. This paper attempts to quantitatively describe the effects of different physical properties on the critical diameter of bubble detachment by combining the reported equations and dynamic computational models.

The impacts of temperature and current density were also investigated for a detailed understanding about how the operating conditions for OER affect bubble departure sizes (Figure 2a−d). Figure 2e shows the relationship between bubble detachment diameters and operating conditions, i.e., current density and temperature. The critical departure size of bubbles increases with increasing current density. At room temperature, the bubble diameter was 83 μm at 10 mA cm^{-2} and 280 μm at 400 mA cm^{-2}. The increase in bubble sizes could be explained by the higher interfacial tension force at a higher current density.[27,28] It was reported that surface tension is a function of the electric field.[28] Therefore, the increased voltage at a higher current density will result in higher local surface tension. A greater interfacial tension force, imposed on the bubbles toward the electrode, leads to a larger bubble departure size. From a dynamic perspective, detaching from the electrode surface causes bubbles to induce convection and turbulence in the electrolyte. A stronger drag force will be imposed on bubbles due to the convection. It has also been reported that part of bubble departure occurs with the coalescence of two neighboring bubbles.[29] An increase in the number of bubbles also causes higher frequencies of coalescence and stronger convection. Detached bubbles create a small velocity field near the electrode surface, resulting in a velocity difference between the electrolyte and attached bubbles. This velocity difference will impose a drag force, which is added to the buoyancy force to overcome the interfacial tension force.[30] Both convection and coalescence involve interactions among multiple bubbles, but this paper only considers the effect of the electrolyte solution on the detachment of a single bubble in the following discussion. The effect of temperature can be obtained by comparing the detachment radius of bubbles at 353 and 298 K. For example, at a current density of 200 mA cm^{-2}, the average diameter of 298 K is 210 μm, which is larger than that of 353 K (150 μm). This trend can be explained by dynamic viscosity changes (vide infra).

A comparison on physical properties affected by the temperature shows that dynamic viscosity decreases significantly with increasing temperature (Figure S3). The effect of dynamic viscosity on the bubble detachment radius will be further elaborated using three-dimensional dynamic simulations.

Quantitative Discussions Using Analytical Expressions. The detachment process of a bubble is a function of many factors, including the physical properties of the electrolyte, the surface chemistry of the electrode, and operating conditions.[31] Traditional analysis of detachment is derived from two main forces imposed on a static bubble: buoyancy force and surface tension force. Following this analysis, one of the most classic correlations was proposed by Fritz, which can predict the bubble departure diameter on an ideally flat surface (eq 1).[13,22] However, the surface of nickel electrodes should not be perfectly flat—especially after OER—because the metal turns to metal (hydr)oxide during the oxidation and reconstruction. SEM images of the Ni electrode surface in Figure S4 showed a fence-like structure, indicating a rough surface and consistent with the imperfect surface assumption of Li's model. Based on Fritz's model, Li et al. successfully deduced the analytical equation to predict the

https://doi.org/10.1021/acs.langmuir.2c03488
Langmuir 2023, 39, 4993−5001

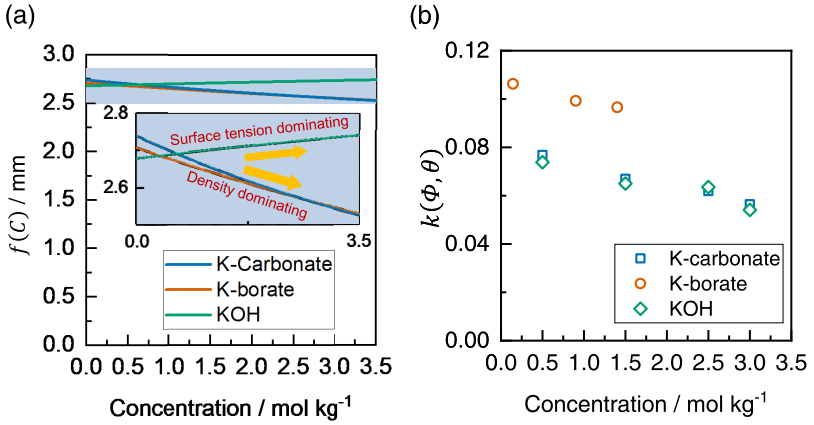

Figure 3. Comparison of the reported equation and experimental results. (a) Relationship between $f(C)$ and solute concentrations. The line is calculated from the linear relationship between the solute concentrations, surface tensions, and liquid densities at 298 K (Figure S2). (b) Relationship between solute concentrations and $k(\Phi,\theta)$, which was obtained from eq 4 using $f(C)$ in panel (a) and the measured average bubble diameters in various solutions at 50 mA cm^{-2} and 298 K are shown in Figure 1e.

bubble diameter on micropillar surfaces, as shown in eq 1.[19] Therefore, we expect that Li's model, which considers the roughness of the electrode surface, will be more suitable to analyze these experimental results than Fritz's formula in a stagnant electrolyte.[13]

$$D = [12r_0 \sin\theta]^{1/2}\left[\frac{\sigma}{g(\rho_l - \rho_v)}\right]^{1/3} \quad (1)$$

Here, D is the bubble detachment size, θ is the intrinsic contact angle, σ is the surface tension, g is the gravitational acceleration, ρ_l is the liquid density, ρ_v is the vapor density, and r_0 is the radius of the pinning area.

To validate our bubble observations and investigate the relationship between electrolyte properties and the diameter of bubbles, Li's equation for predicting bubble detachment size, D^*, on a hemiwicking state was used as expressed in eq 2.

$$D^* = \Phi^{1/4}\sqrt{\frac{6\sqrt[3]{4}\,\sin\theta\,\sin\theta_l^*}{(2 + 3\cos\theta_l^* - \cos^3\theta_l^*)^{1/3}}}\left[\frac{\sigma}{g(\rho_l - \rho_v)}\right]^{1/2} \quad (2)$$

Here, Φ is the solid fraction, and θ_l^* is the corresponding equilibrium apparent contact angle for a hemiwicking state.

The solid fraction and the corresponding equilibrium apparent contact angle for a hemiwicking state are given by eqs 3 and 4.

$$\Phi = \frac{d^2}{(d + p)^2} \quad (3)$$

$$\cos\theta_l^* = \Phi\cos\theta + (1 - \Phi) \quad (4)$$

where d is the width of the micropillar and p is the pitch distance of the micropillar of a rectangular shape. To simplify, Li's equation is separated into two parts as shown in eqs 5 and 6.

$$\text{electrode term: } k(\Phi, \theta) = \Phi^{1/4}\sqrt{\frac{6\sqrt[3]{4}\,\sin\theta\,\sin\theta_l^*}{(2 + 3\cos\theta_l^* - \cos^3\theta_l^*)^{1/3}}} \quad (5)$$

$$\text{electrolyte term: } f(C) = \left[\frac{\sigma(C)}{g(\rho_l(C) - \rho_v)}\right]^{1/2} \quad (6)$$

The solid fraction and apparent contact angle are properties highly related to the electrode surface, and thus, eq 5 can be viewed as a function reflecting the electrode. As for the remaining part, the surface tension and the liquid phase density are two physical properties solely related to the electrolyte. Therefore, eq 6 can be viewed as a function reflecting the physical properties of the electrolyte. In this analytical expression, we note that the influence of electrolytes and electrodes on the critical diameter of bubble departure can be separated as $f(C)$ and $k(\Phi,\theta)$.

The potential impact of the electrolyte on the electrode surface has been included as a change of solid fraction and apparent contact angle. For instance, during the oxygen evolution reaction, a NiO_X layer would be formed at the surface of the nickel plate, thus changing the hydrophilicity of the electrode, the surface roughness, and thus, the resulting apparent contact angle. In the bubble observation experiments, average bubble departure sizes were found to be smaller in a denser electrolyte solution (Figure 1e). However, discussing the electrolyte contribution of bubble detachment diameters is relatively complicated due to the existence of two variables: surface tension and liquid density. Therefore, it is necessary to correlate these two variables with solute concentration. By measuring the density and surface tension of electrolytes with different concentrations (Figure S2), we found that these physical properties could be expressed as a function of solute concentration within the studied range. The density of the gas phase was considered to be constant due to continuously produced oxygen from OER; thus, the impact of electrolytes on bubble sizes can be directly written as the analytical equation of solute concentration; see eq 6.

The relationship between the solute concentration and $f(C)$ is shown in Figure 3a. In the K-borate buffer solution and K-carbonate buffer solution, the electrolyte part decreases with a higher solute concentration. The different trend between the potassium hydroxide solution and K-carbonate buffer solution might be derived from the slope difference shown in Figure S2. Surface tension varies faster with concentration than density in a potassium hydroxide solution. This results in a situation

https://doi.org/10.1021/acs.langmuir.2c03488
Langmuir 2023, 39, 4993−5001

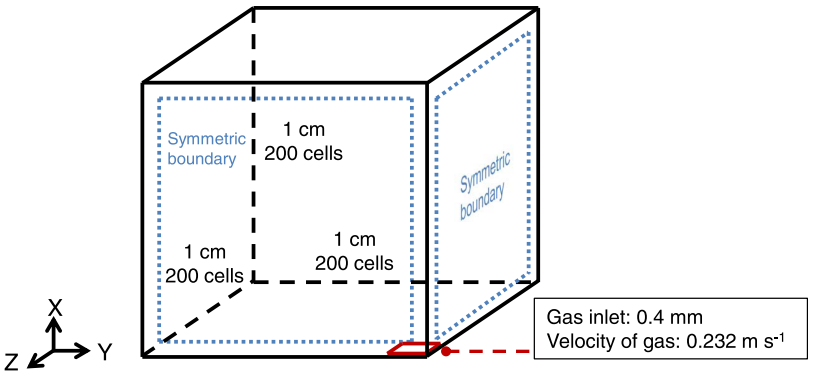

Figure 4. Schematic of the simulation model. Three-dimensional numerical simulation model with two symmetric boundaries. The entire simulation regime is a 1 cm × 1 cm × 1 cm cube with a fine-mesh setting (200 cells × 200 cells × 200 cells).

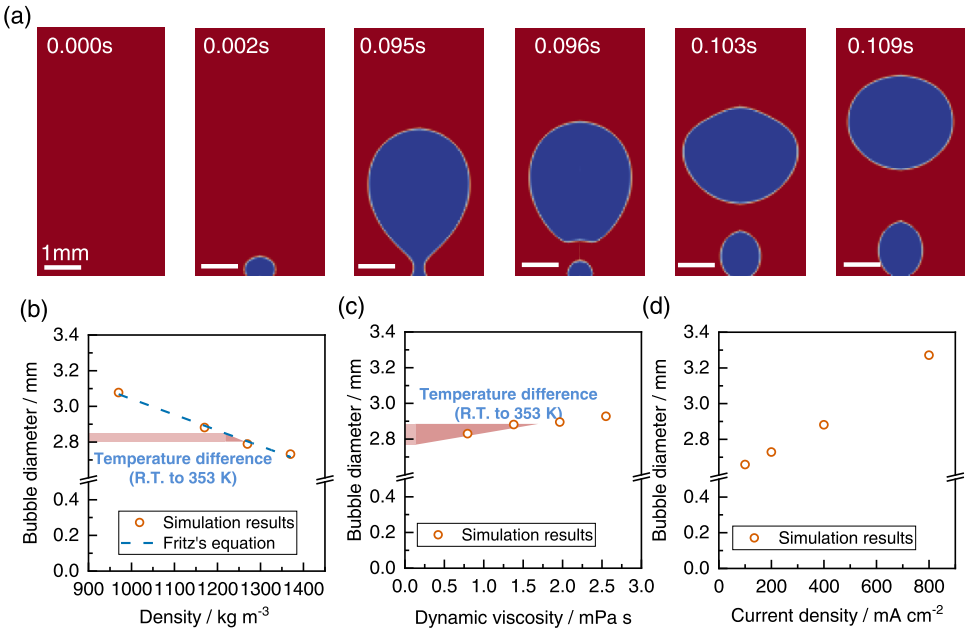

Figure 5. Numerical results from the simulation model. (a) Time-lapse (from 0.000 to 0.109 s) images of the bubble departure process from a flat surface (scale bar is 1 mm). Relationship between bubble departure diameters and (b) density, (c) dynamic viscosity, and (d) current density. These are varied independently in the simulation model as shown in Figure 4.

where different physical properties determine the bubble detachment sizes.

Though the contribution of electrolytes has been elucidated, the bubble diameter predicted from the electrolyte alone had a significant deviation from the experimental results. As a result, one must also examine the electrode part. For each solute concentration (Figure 3b), the contribution of electrodes, $k(\Phi,\theta)$, was determined by dividing the average bubble detachment diameters observed from the experiments (Figure 1e) by the value of $f(C)$ (Figure 3a).

The estimated $k(\Phi,\theta)$ from different electrolyte solutions all show a decreasing trend with solute concentration. Notice that there are two parameters in eq 5 that mainly affect the contribution of the electrode part: the solid fraction and the contact angle. Both have a positive impact on the contribution of the electrode, and thus, the declining trend may be due to the reduction in solid fraction, the reduction of contact angles, or both. The definition of solid fraction in the analytical expression comes from the micropillar surface, and the nickel plate applied in the experiment did not possess such a perfectly uniform surface structure. The reduction in the solid fraction can only be abstractly understood, where the electrode surface topography becomes rougher. The decrease in the contact angles indicates that the electrode becomes more hydrophilic.

These changes indicate that the surface's hydrophilicity or morphology is quite different after performing OER in various solute concentrations of electrolytes. To clarify, the apparent contact angles were measured after performing OER on fresh nickel electrodes in various concentrations of electrolytes at 20 mA cm^{-2} for 30 min. The apparent contact angles decreased with higher solute concentrations shown in Figures S5 and S6. This demonstrates that the electrode surfaces are increasingly hydrophilic. This observation strongly supports the inference from eq 5. We also find that the influence of the electrode part is more significant and plays a decisive role upon comparing the influence of electrolytes and electrodes.

Dynamic Three-Dimensional Simulation. The above discussion is based on experimental observations and Li's analytical expression. The findings demonstrate the effect of electrolyte physical parameters, such as liquid phase density and surface tension, on the departure diameters of bubbles as well as the potential effect of the electrode surface affected by

https://doi.org/10.1021/acs.langmuir.2c03488
Langmuir 2023, 39, 4993−5001

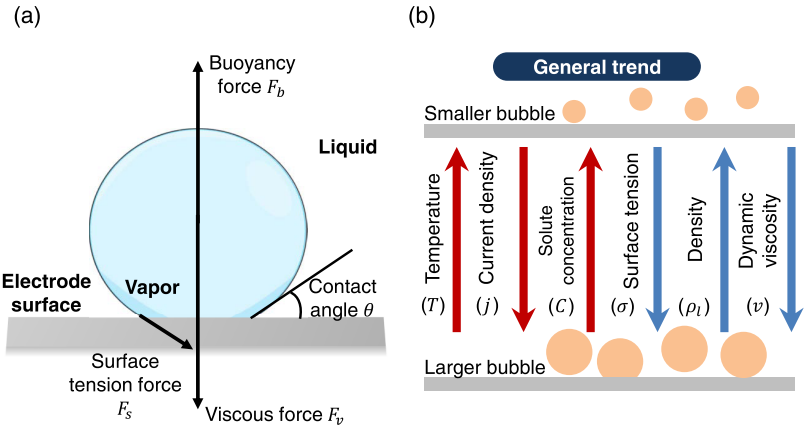

Figure 6. (a) Schematic of forces on bubbles during the detachment. (b) General trends between operating conditions and bubble diameter. The red arrow represents those parameters that can be tuned during experimental operation and the blue arrow represents those physical parameters of electrolytes. The direction of the arrows indicates the effect of increasing such a property on bubble diameters.

the OER. By correlating the liquid phase density and surface tension with the solute concentration, the relationship between the bubble departure sizes and the electrolyte concentration was quantitatively described. The phenomenon whereby high-concentration electrolyte solutions induce smaller bubble sizes was explained.

However, these discussions are limited to the static parameters of the electrolyte and electrodes. Neither Fritz's model nor Li's analytical expression can explain bubble behavior under higher current densities and the temperature dependence. For example, higher applied current density was found to induce larger bubbles at a given electrolyte and operating temperature (Figure 2e). This phenomenon cannot be explained by the difference in density or surface tension, because the dynamic deformation of the fluids is not considered in the force balance.

In addition to the electrolyte density, surface tension, and hydrophilicity of the electrode surface, there are many other dynamic parameters that will affect this process such as dynamic viscosity and gas inlet velocity. Therefore, the decrease of dynamic viscosity at elevated temperatures and higher gas inlet velocity at high current densities need to be investigated further. In this simulation study, the gas inlet velocity was introduced as the controllable parameter representing current density, as higher current densities will increase the oxygen evolution rate. To investigate the effect of temperature and current density, a three-dimensional volume and fluid simulation model of an oxygen bubble evolving in the aqueous solutions was built (Figure 4). To simulate the complete process of bubble generation and detachment, the liquid phase was set in the whole model at the initial state. These processes were simulated via the volume of fluid (VOF) method based interFoam solver shipped with OpenFOAM-9 by solving the Navier–Stokes equations.[32] (Detailed governing equations are shown in the Supporting Information.) A quarter of the sphere was considered with symmetry boundaries to reduce the computational cost. Figure 5a shows the time-lapse images of the bubble departure process from a flat surface, where the gas inlet velocity was converted from the current density. (A detailed explanation of the conversion is shown in the Supporting Information). The contact line was always pinned from the initial state with a contact angle of 30°. To verify the feasibility of the model, we next compared it to Fritz's formula, which predicts the bubble detachment diameter on flat surfaces and quiescent liquid with varied liquid densities and surface tensions[13] (Figure 5b). Note that this numerical model was not solving the Fritz's equations but the governing equations shown in eqs S3–S5, which made it reasonable to compare their results. Bubble diameters predicted by the model under different densities are close to the calculation result of the analytical expression. It is worth noting that here, we compared our simulation results with Fritz's model instead of Li's model. Though these two models assume differently on the electrode surface, where Li's model takes the textured surface and different wetting states into consideration, and Fritz's model merely describes a perfectly smooth surface, they are compatible with the electrolyte contribution. Therefore, it is reasonable to utilize Fritz's expression to verify this simulation model. Besides, our simulation model is taking more dynamic parameters into consideration to describe the detachment process of bubbles, while Fritz's model only considers the physical properties of liquid and gas, such as density, surface tension, and hydrophilicity.

At the same time, bubble sizes under different surface tensions were also predicted, and the results are similar to Fritz's model (Figure S7), thus indicating that this model is valid and can be utilized to predict the effects of dynamic viscosity and current density.

Figure 5c shows that the increase in dynamic viscosity can cause a slight increase in the departure diameters. The viscous force formed by the dynamic deformation works against the buoyancy force, thus requiring larger bubble sizes to detach. This partially explains the phenomenon whereby bubble sizes were found to be smaller at higher temperatures. Highlighted regions, shown in Figure 5b,c, demonstrate the contribution of density and dynamic viscosity separately when the temperature changed from R.T. (298 K) to 353 K. The liquid viscosity decreases by elevating the temperature, thus reducing the detachment size of the bubbles, while the liquid density remains nearly unchanged. The current density was converted to the gas inlet velocity in the model to investigate its effect on bubble behavior. A higher current density corresponds to a faster gas inlet velocity. Figure 5d shows that an increase in the inlet velocity can significantly increase the simulated bubble departure sizes similar to the observed increase in the bubble diameters at a high current density in the experiment. A higher applied current density leads to a higher deformation rate of

https://doi.org/10.1021/acs.langmuir.2c03488
Langmuir 2023, 39, 4993–5001

fluids and a higher resulting viscous force. This in turn results in a larger detachment size. The simulation results of the model offer additional design guidelines beyond the common analytical expressions for predicting the bubble size, such as Fritz's model and Li's equation. There are still missing dynamic factors in the water electrolysis that also impact the bubble detachment diameters. (The forces considered here during detachment are shown in Figure 6a.) For instance, convection formed by other bubble departures and coalescence with neighboring bubbles will also contribute to the detachment. However, the three-dimensional model initially established a quantitative relationship between current density, dynamic viscosity, and bubble departure diameters.

The schematic of forces on bubbles in Figure 6a shows that buoyancy force works toward the electrolyte while surface tension force and viscous force work toward the electrode. Their balance should determine the detachment bubble size. The general trends summarized from the experimental data and numerical simulation are shown in Figure 6b. Elevating the temperature significantly reduces the dynamics viscosity and the resultant viscous force, leading to smaller bubbles. Meanwhile, a higher current density increases the deformation rate of fluids and the resultant viscous force, leading to larger bubbles. The data show the rough direction of bubble diameter change under different operating conditions.

CONCLUSIONS

We quantitatively investigated how electrolyte solutions impact bubble departure diameters due to their physical properties and the electrode surface exposed to the electrochemical reactions. Upon combination with analytical static equations and experimental evidence, we separately analyzed the impact of electrolyte density and surface tension on bubble behavior by deducing equations and constructing a quantitative relationship from them. This quantitative description indicates that a higher electrolyte concentration induces a smaller bubble diameter. The dominating physical parameter differs depending on the nature of the electrolyte solution. The effect of electrolytes and electrodes on bubbles was studied: We found that the electrode surface, which altered during the reaction, was more important for bubble detachment than the electrolyte. In addition, a three-dimensional numerical simulation model was constructed to investigate the dynamic effects during the bubble growth. This model successfully depicts the entire process of bubble detachment and is validated by Fritz's model. By simulating different dynamic viscosities and inlet velocities, we found that an increase in dynamic viscosity could slightly increase the bubble sizes while a higher inlet velocity could significantly increase the bubble sizes. Our work provides a theoretical basis for attempts to regulate bubbles by electrolyte engineering. The numerical simulation provides additional insights into the bubble detachment process. Future studies require a deep investigation into the effect of the electrolyte on the hydrophilicity and morphology of the electrode surface.

EXPERIMENTAL SECTION

Chemicals. All chemicals were purchased from Sigma-Aldrich: KOH (>85%), H_3BO_3 (99.9%), H_3PO_4 (99.99%), and $KHCO_3$ (>95%). Nickel plates and Pt wires were purchased from Nilaco Corporation. O_2 (99.99995%) gases were used.

Electrolyte Preparation. The electrolyte solutions were prepared via several steps. First, the buffering compound was weighed and dissolved in ultrapure water according to the concentration. The pH was adjusted by adding 5 mol kg^{-1} KOH solutions until the pH reached 10.5.

Electrochemical Measurement and Characterization. A three-electrode configuration was utilized for electrochemical measurements during the bubble observation experiments. Chronopotentiometry (CP) was performed in the three-electrode system during the high-speed camera recording of oxygen detachment. CP used a Pt wire as the counter electrode, a bent Ni plate (Nilaco Corporation) as the working electrode, and $Hg/HgCl_2$ (saturated with KCl, BAS, Inc.) as the reference electrode using a 16-channel research-grade potentiostat system (VMP3, BioLogic Science Instruments). O_2 gas was continuously supplied to the cell to saturate oxygen in the electrolyte solutions before and during all bubble observation experiments.

The droplet contact angles were measured with a high-speed camera (Phantom VEO710L, Vision Research Inc.). Here, a 0.3 μL of ultrapure water droplet was dropped on the surface of nickel plates prepared under 20 mA cm^{-2} for 30 min. ImageJ was used to calculate bubble contact angles with the contact angle plugins. The densities and viscosities of the electrolyte buffer solutions were measured with a viscometer (Stabinger viscometer SVM 2001, Anton Paar). Surface tensions of electrolyte buffer solution were measured through a capillary rise method using a dyne gauge (DG-1, Surfgauge Instruments).

Bubble Detachment Observation. Oxygen bubbles detaching at the bent line of the working electrodes were recorded by a high-speed camera and a long working distance lens (VW-600M and VH-250L, Keyence Co.). The field of view was 640 × 480 pixels with a recording rate of 500 frames/s and an exposure time of 1 μs.

Three-Dimensional Numerical Simulation. The processes of the bubble generation and detachment were simulated through the volume of fluid (VOF) method in openFOAM.[32] (Detailed governing equations are shown in the Supporting Information.) The entire simulation region is 1 cm × 1 cm × 1 cm cube with a fine-mesh setting (200 cells × 200 cells × 200 cells). This was validated via a mesh study (Figure S8). The symmetry boundary condition was used to model the bubble behaviors. The open boundary condition was applied to the inlet of gas and the top of the regime, and the wall boundary condition was applied to the rest of the boundaries of the simulation domain. (For the wall boundary, the velocity field was set as no slip and the pressure field was set as fixed flux pressure, which meant that the value of pressure gradient was specified by the velocity field and a static contact angle was imposed as 30°.)

ASSOCIATED CONTENT

Supporting Information

The Supporting Information is available free of charge at https://pubs.acs.org/doi/10.1021/acs.langmuir.2c03488.

> Experimental setup and detailed illustration of the bent Ni plate; relationship between physical properties and concentration of different electrolytes; physical properties at different temperatures; SEM images and the apparent contact angle tests related to Ni plate surfaces; mesh study; detailed governing equations of 3D numerical simulation; conversion from current density to gas inlet velocity (PDF)

AUTHOR INFORMATION

Corresponding Author

Kazuhiro Takanabe − *Department of Chemical System Engineering, School of Engineering, The University of Tokyo, Tokyo 113-8656, Japan;* orcid.org/0000-0001-5374-9451; Email: Takanabe@chemsys.t.u-tokyo.ac.jp

https://doi.org/10.1021/acs.langmuir.2c03488
Langmuir 2023, 39, 4993−5001

Authors

Huihang Qiu − *Department of Chemical System Engineering, School of Engineering, The University of Tokyo, Tokyo 113-8656, Japan*

Keisuke Obata − *Department of Chemical System Engineering, School of Engineering, The University of Tokyo, Tokyo 113-8656, Japan*

Zhicheng Yuan − *Department of Mechanical Engineering, School of Engineering, The University of Tokyo, Tokyo 113-8656, Japan;* orcid.org/0000-0001-8599-8743

Takeshi Nishimoto − *Department of Chemical System Engineering, School of Engineering, The University of Tokyo, Tokyo 113-8656, Japan*

Yaerim Lee − *Department of Mechanical Engineering, School of Engineering, The University of Tokyo, Tokyo 113-8656, Japan*

Keisuke Nagato − *Department of Mechanical Engineering, School of Engineering, The University of Tokyo, Tokyo 113-8656, Japan*

Ikuya Kinefuchi − *Department of Mechanical Engineering, School of Engineering, The University of Tokyo, Tokyo 113-8656, Japan;* orcid.org/0000-0003-1680-5981

Junichiro Shiomi − *Department of Mechanical Engineering, School of Engineering, The University of Tokyo, Tokyo 113-8656, Japan;* orcid.org/0000-0002-3552-4555

Complete contact information is available at: https://pubs.acs.org/10.1021/acs.langmuir.2c03488

Author Contributions

H.Q., K.O., T.N., and K.T. designed the research. H.Q., T.N., and Y.L. performed the experiments. H.Q., K.O., and Z.Y. performed the numerical simulations. H.Q., K.O., Z.Y., T.N., Y.L., I.K., J.S., and K.T. analyzed the data. H.Q. wrote the first draft of manuscript. All authors helped revise the article and approved the contents. K.N., I.K., J.S., and K.T. acquired funding. K.T. supervised the project.

Notes

The authors declare no competing financial interest.

■ ACKNOWLEDGMENTS

This work was supported by MEXT Program: Data Creation and Utilization-Type Material Research and Development Project Grant Number JPMXP1122712807. H.Q. thanks the University of Tokyo Fellowship.

■ REFERENCES

(1) Zhang, H.; Maijenburg, A. W.; Li, X.; Schweizer, S. L.; Wehrspohn, R. B. Bifunctional Heterostructured Transition Metal Phosphides for Efficient Electrochemical Water Splitting. *Adv. Funct. Mater.* **2020**, *30*, No. 2003261.

(2) Dukovic, J.; Tobias, C. W. The influence of attached bubbles on potential drop and current distribution at gas-evolving electrodes. *J. Electrochem. Soc.* **1987**, *134*, 331.

(3) Gabrielli, C.; Huet, F.; Keddam, M.; Macias, A.; Sahar, A. Potential drops due to an attached bubble on a gas-evolving electrode. *J. Appl. Electrochem.* **1989**, *19*, 617−629.

(4) Leistra, J. A.; Sides, P. J. Voltage components at gas evolving electrodes. *J. Electrochem. Soc.* **1987**, *134*, 2442. German, S. R.; Edwards, M. A.; Ren, H.; White, H. S. Critical Nuclei Size, Rate, and Activation Energy of H2 Gas Nucleation. *J. Am. Chem. Soc.* **2018**, *140*, 4047−4053.

(5) Dorfi, A. E.; West, A. C.; Esposito, D. V. Quantifying Losses in Photoelectrode Performance Due to Single Hydrogen Bubbles. *J. Phys. Chem. C* **2017**, *121*, 26587−26597.

(6) Iwata, R.; Zhang, L.; Wilke, K. L.; Gong, S.; He, M.; Gallant, B. M.; Wang, E. N. Bubble growth and departure modes on wettable/non-wettable porous foams in alkaline water splitting. *Joule* **2021**, *5*, 887−900.

(7) Angulo, A.; van der Linde, P.; Gardeniers, H.; Modestino, M.; Rivas, D. F. Influence of Bubbles on the Energy Conversion Efficiency of Electrochemical Reactors. *Joule* **2020**, *4*, 555−579.

(8) Wang, J.; Yang, Q.; Wang, M.; Wang, C.; Jiang, L. Rose petals with a novel and steady air bubble pinning effect in aqueous media. *Soft Matter* **2012**, *8*, 2261−2266.

(9) Hine, F.; Murakami, K. Bubble effects on the solution IR drop in a vertical electrolyzer under free and forced convection. *J. Electrochem. Soc.* **1980**, *127*, 292.

(10) Vogt, H. The problem of the departure diameter of bubbles at gas-evolving electrodes. *Electrochim. Acta* **1989**, *34*, 1429−1432.

(11) Ahn, S. H.; Hwang, S. J.; Yoo, S. J.; Choi, I.; Kim, H.-J.; Jang, J. H.; Nam, S. W.; Lim, T.-H.; Lim, T.; Kim, S.-K.; Kim, J. J. Electrodeposited Ni dendrites with high activity and durability for hydrogen evolution reaction in alkaline water electrolysis. *J. Mater. Chem.* **2012**, *22*, 15153−15159.

(12) Modestino, M. A.; Hashemi, S. M. H.; Haussener, S. Mass transport aspects of electrochemical solar-hydrogen generation. *Energy Environ. Sci.* **2016**, *9*, 1533−1551.

(13) Duhar, G.; Colin, C. Dynamics of bubble growth and detachment in a viscous shear flow. *Phys. Fluids* **2006**, *18*, No. 077101.

(14) Lin, M.-Y.; Hourng, L.-W.; Kuo, C.-W. The effect of magnetic force on hydrogen production efficiency in water electrolysis. *Int. J. Hydrogen Energy* **2012**, *37*, 1311−1320.

(15) Rivas, D. F.; Cintas, P.; Gardeniers, H. J. Merging microfluidics and sonochemistry: towards greener and more efficient micro-sono-reactors. *Chem. Commun.* **2012**, *48*, 10935−10947.

(16) Esposito, D. V. Membraneless Electrolyzers for Low-Cost Hydrogen Production in a Renewable Energy Future. *Joule* **2017**, *1*, 651−658. Hadikhani, P.; Hashemi, S. M. H.; Schenk, S. A.; Psaltis, D. A membrane-less electrolyzer with porous walls for high throughput and pure hydrogen production. *Sustainable Energy Fuels* **2021**, *5*, 2419−2432.

(17) Brussieux, C.; Viers, P.; Roustan, H.; Rakib, M. Controlled electrochemical gas bubble release from electrodes entirely and partially covered with hydrophobic materials. *Electrochim. Acta* **2011**, *56*, 7194−7201.

(18) Li, Y.; Zhang, H.; Xu, T.; Lu, Z.; Wu, X.; Wan, P.; Sun, X.; Jiang, L. Under-Water Superaerophobic Pine-Shaped Pt Nanoarray Electrode for Ultrahigh-Performance Hydrogen Evolution. *Adv. Funct. Mater.* **2015**, *25*, 1737−1744.

(19) Li, J.; Gong, S.; Zhang, L.; Cheng, P.; Ma, X.; Hong, F. Wetting States and Departure Diameters of Bubbles on Micro-/Nano-structured Surfaces. *Langmuir* **2022**, *38*, 3180−3188.

(20) Ma, D.; Liu, M.; Zu, Y.; Tang, C. Two-dimensional volume of fluid simulation studies on single bubble formation and dynamics in bubble columns. *Chem. Eng. Sci.* **2012**, *72*, 61−77.

(21) Albadawi, A.; Donoghue, D. B.; Robinson, A. J.; Murray, D. B.; Delauré, Y. M. C. On the analysis of bubble growth and detachment at low Capillary and Bond numbers using Volume of Fluid and Level Set methods. *Chem. Eng. Sci.* **2013**, *90*, 77−91.

(22) Fritz, W. Maximum volume of vapour bubbles. *Phys. Z.* **1935**, *36*, 379−384.

(23) van der Linde, P.; Peñas-López, P.; Moreno Soto, Á.; van der Meer, D.; Lohse, D.; Gardeniers, H.; Rivas, D. F. Gas bubble evolution on microstructured silicon substrates. *Energy Environ. Sci.* **2018**, *11*, 3452−3462.

(24) Shinagawa, T.; Ng, M. T. K.; Takanabe, K. Electrolyte engineering towards efficient water splitting at mild pH. *ChemSusChem* **2017**, *10*, 4155−4162.

(25) Nishimoto, T.; Shinagawa, T.; Naito, T.; Takanabe, K. Delivering the Full Potential of Oxygen Evolving Electrocatalyst by Conditioning Electrolytes at Near-Neutral pH. *ChemSusChem* **2021**, *14*, 1554−1564.

(26) Komiya, H.; Shinagawa, T.; Takanabe, K. Electrolyte Engineering for Oxygen Evolution Reaction Over Non-Noble Metal Electrodes Achieving High Current Density in the Presence of Chloride Ion. *ChemSusChem* **2022**, *15*, No. e202201088.
(27) Zhang, D.; Zeng, K. Evaluating the Behavior of Electrolytic Gas Bubbles and Their Effect on the Cell Voltage in Alkaline Water Electrolysis. *Ind. Eng. Chem. Res.* **2012**, *51*, 13825−13832.
(28) Lubetkin, S. The motion of electrolytic gas bubbles near electrodes. *Electrochim. Acta* **2002**, *48*, 357−375.
(29) Iwata, R.; Zhang, L.; Lu, Z.; Gong, S.; Du, J.; Wang, E. N. How Coalescing Bubbles Depart from a Wall. *Langmuir* **2022**, *38*, 4371−4377.
(30) Taqieddin, A.; Nazari, R.; Rajic, L.; Alshawabkeh, A. Review-Physicochemical hydrodynamics of gas bubbles in two phase electrochemical systems. *J. Electrochem. Soc.* **2017**, *164*, E448−E459.
(31) Kulkarni, A. A.; Joshi, J. B. Bubble formation and bubble rise velocity in gas− liquid systems: a review. *Ind. Eng. Chem. Res.* **2005**, *44*, 5873−5931.
(32) Hirt, C. W.; Nichols, B. D. Volume of fluid (VOF) method for the dynamics of free boundaries. *J. Comput. Phys.* **1981**, *39*, 201−225.

https://doi.org/10.1021/acs.langmuir.2c03488
Langmuir 2023, 39, 4993−5001